Electronic Supplementary Information

Dynamic Charge Collecting Mechanisms of Cobalt Phosphate on Hematite Photoanode Studied by Photoinduced Absorption Spectroscopy

Dongfeng Li,[ab] Ruifang Wei,[ac] Heng Yin,[a] Hemin Zhang,[d] Xiuli Wang,[a]* and Can Li[abc]*

[a]State Key Laboratory of Catalysis, Dalian Institute of Chemical Physics, Chinese Academy of Sciences, Dalian National Laboratory for Clean Energy, Dalian 116023, China.

[b]University of Chinese Academy of Sciences, Beijing 100049, China

[c]Department of Chemical Physics, University of Science and Technology of China, Hefei 230026, China

[d]College of Materials Science and Engineering, Sichuan University, Engineering Research Center of Alternative Energy Materials and Devices, Ministry of Education, Chengdu 610065, China

Table of Contents

Experimental section

All the reagents are used as received without further purification. All aqueous solutions including sample preparation and electrolytes were prepared with deionized pure water (> 18.2 MΩ/cm). Unless mentioned otherwise, all of the experiments were conducted under normal atmospheric conditions.

Sample preparation

Preparation of FeOOH films. FeOOH films were prepared by solvothermal deposition method.[1] The substrates of FTO (1.5 cm × 2 cm, Nippon Sheet Glass Company, Japan) were firstly cleaned in acetone, isopropanol, ethanol and deionized water for 20 min respectively. The clean FTO was attached with tape on the glass side and placed leaned against the wall of the vessel. Afterwards, 50 mL solution containing 0.1 M $FeCl_3$•$6H_2O$ and 0.225 M $CO(NH_2)_2$ (dense sample) or 1 M $NaNO_3$ (porous sample) was added. Then it the vessel was sealed and placed in the oven at 100 ^oC for 4 h. Finally, the deposited FeOOH film was washed by deionized water.

Surface doping with tin. For the surface doping of Sn, firstly 0.1 M $SnCl_2$ ethanol solution was prepared by dissolving 0.9024 g $SnCl_2$•$2H_2O$ in 40 mL absolute ethanol. Then the FeOOH film was immersed in the solution for 10 min.[2] Finally, the electrode was swept to dry by compressed air, and annealed at 550 ^oC for 3 h, followed by heat treatment at 750 ^oC for 15 min. The as-obtained dense samples were labeled as Fe_2O_3. The as-obtained porous samples were labeled as porous-Fe_2O_3.

Deposition of CoPi overlayer. Electrodeposition of CoPi overlayer on FTO, Fe_2O_3, and porous-Fe_2O_3 photoelectrodes was carried out by modified procedures published elsewhere.[3] The employed electrolyte contained 0.5 mM $Co(NO_3)_2$•$2H_2O$ in

0.1 M phosphate buffer (pH 6.77). The working electrode was subjected to 1.6 V_{RHE} with 5 min. The obtained samples were denoted as CoPi, CoPi/Fe_2O_3 and CoPi/porous-Fe_2O_3.

Deposition of NiOOH overlayer. Electrodeposition of NiOOH overlayer on Fe_2O_3 photoelectrode or FTO was prepared by reported electrodeposition methods[4] with solution of 0.1 M NaOAc with 16 mM NiOAc. Electrodeposition was performed five times by consecutive linear sweeps from 1.7 to 2.0 V_{RHE} at 10 mV/s. The obtained samples were named as NiOOH and NiOOH/Fe_2O_3.

Regulation of oxygen vacancy for hematite photoanode.[5] For decreasing oxygen vacancy, as-prepared Fe_2O_3 was annealed at 600 ^oC for 2 h in air, which is named as Fe_2O_3-air. In order to increase oxygen vacancy, as-prepared Fe_2O_3 was annealed at 600 ^oC for 2 h in pure argon flow in a tube furnace. The obtained sample was denoted as Fe_2O_3-Ar. After CoPi modification on hematite photoanodes of regulating oxygen vacancy, they were noted as CoPi/Fe_2O_3-air and CoPi/Fe_2O_3-Ar.

Surface doping with fluorine.[6] Fe_2O_3 film was immersed in 0.05 M NaF solution for 10 min, followed calcination at 400 ^oC for 30 min in furnace. The obtained samples were termed as F-Fe_2O_3.

Tantalum doping and constructing homojunction. The preparation processes of high-performance homojunction samples (Fe_2O_3/Ta-Fe_2O_3) were coincident with our previous work.[7]

Insulator modification with SnO_2.[8] Fe_2O_3 film was immersed in 0.02 M $SnCl_4$•$5H_2O$ and 1 M $CO(NH_2)_2$ solution and deposited for 20 min at 100 ^oC in the oven, followed calcination at 500 ^oC for 2 h in furnace. The prepared samples were

named as SnO_2/Fe_2O_3.

Photoelectrochemcial (PEC) measurements

The electrolyte for PEC or electrochemical water oxidation measurements was 1 M NaOH aqueous solution (pH 13.7). A three-electrode setup controlled by a CHI 760C potentiostat was employed with Fe_2O_3 as the working electrode, Ag/AgCl/saturated KCl (Ag/AgCl) as the reference electrode, and Pt foil as the counter electrode. Potentials measured versus Ag/AgCl were converted to reversible hydrogen electrode (RHE), $E_{RHE} = E_{Ag/AgCl} + 0.1981\ V + 0.0591\ V \bullet pH$. Unless mentioned otherwise, all of the potentials were versus RHE. The photoelectrodes were illuminated from the electrolyte-electrode interface.

Electrochemical impedance spectroscopy (EIS) of photoelectrodes under illumination and dark were carried out using an electrochemical workstation (VersaSTAT MC) from 10^5 Hz to 10^{-1} Hz with a signal amplitude of 10 mV.

Cyclic voltammetry (CV) with various scan rates and open circuit potential (OCP) with chopped light of photoelectrodes were conducted by a CHI 760C potentiostat.

Photoinduced absorption (PIA) spectroscopy

The PIA spectroscopy was performed using long-pulsed (≈ s) LED light source to generate photoinduced charges in the photoanode.[9] The interval of light on/light off was controlled by a wavefunction generator (0.09 Hz and 50 % duty ratio), which simultaneously sent a trigger signal to oscilloscope (Tektronics TDS 2012c) and DAQ card (National Instruments NI USB-6211). During collecting PIA spectra, the illumination duration was ~5 s, followed by ~5 s in the dark. Meanwhile, a monochromatic probe light (for example, 694.3 nm) from a tungsten halogen lamp

(Bentham IL1 Tungsten Halogen lamp) was used to monitor the photogenerated charges dynamics on photoelectrode.[3] The optical density difference (ΔOD) of probe light was monitored using a Si photodiode detector (Hamamatsu S3071). A potentiostat (CHI 760C) was used to provide a constant applied potential and collect the transient photocurrent data.

Electroinduced absorption (EIA) spectroscopy

When collecting EIA spectroscopy, the potential pulse instead of light pulse in PIA spectroscopy was applied to induce the absorption variation. After the electrode was stabilized ~20 s under constant potential using chronoamperometry, the absorption spectra were recorded. SECA spectrum is the difference of absorption spectra under two potentials.

Spectroelectrochemical absorption (SECA) spectroscopy

When collecting SECA spectroscopy,[10] the potential instead of light was applied to induce the absorption variation. After the electrode was stabilized ~20 s under constant potential using chronoamperometry (V650, Jasco), the absorption spectra were recorded. SECA spectrum is the difference of absorption spectra under two potentials.

Transient absorption spectroscopy (TAS) and transient photocurrent (TPC)

TAS and TPC measurements were carried out using the third harmonic of a Nd:YAG laser (Opolette HE-355-LD, 355 nm, 7 ns pulse width, 1.05 s period) as the pump light. A liquid light guide transmitted the laser pulse to the sample resulting in an incident pump intensity of ca. 225 μJ/pulse (355 nm). A 100 W tungsten lamp (Bentham, IL 1) coupled to a monochromator (Zolix, Omni - λ 300) was used as the

probe light. Variation in optical density (ΔOD) of the sample was calculated by measuring the transmitted light using a Si photodiode (Hamamatsu) and an amplification system coupled to both an oscilloscope (Tektronix, TDS 2012C) and data acquisition card (National Instruments NI-6221). The data were averaged over 300 laser shots. The operando TAS and TPC experiments were implemented by three-electrode setup controlled by a CHI 760C potentiostat in 1M NaOH solution (pH = 13.7), with the photoanode, Pt, and Ag/AgCl as working, counter and reference electrodes, respectively. During TAS and TPC measurements, a constant potential was maintained by chronoamperometry.

Table. S1 For PIA results in Fig. 3a and 3c, the accumulation and dissipation lifetimes in Fe_2O_3 and CoPi/Fe_2O_3 photoanodes are calculated and fitted by using mono-exponential and bi-exponential function: $y = y_0 + A_1 \bullet \exp((t-t_0)/\tau_1)$ or $y = y_0 + A_1 \bullet \exp((t-t_0)/\tau_1) + A_2 \bullet \exp((t-t_0)/\tau_2)$, respectively. Y_0 is the intercept. T_0 is initial points of accumulated or dissipative processes. A_1 and A_2 are the amplitudes. τ_1 and τ_2 are fitting lifetimes. The average lifetime of τ_{ave} is calculated by equation: $\tau_{ave} = (A_1 \bullet \tau_1 + A_2 \bullet \tau_2)/(A_1 + A_2)$. A_1, A_2, τ_1 and τ_2 are the parameters in Table S1.

Fe_2O_3								
Potential V_{RHE}	Accumulated lifetime			Dissipative lifetime				
	A_1 (ΔOD)	τ_1 (s)	$\tau_{average}$ (s)	A_1 (ΔOD)	τ_1 (s)	A_2 (ΔOD)	τ_2 (s)	$\tau_{average}$ (s)
0.6	–	–	–	–	–	–	–	–
0.7	–	–	–	–	–	–	–	–
0.8	–	–	–	–	–	–	–	–
0.9	–	–	–	–	–	–	–	–
1.0	−5.48E−5	0.41	0.41	5.03E−5	0.04	4.28E−5	1.28	0.61
1.1	−2.03E−4	0.53	0.53	8.56E−5	0.41	1.06E−4	1.73	1.14
1.2	−3.58E−4	0.54	0.54	6.32E−5	0.20	2.92E−4	1.48	1.25
1.3	−4.13E−4	0.52	0.52	1.03E−4	0.28	3.20E−4	2.11	1.66
1.4	−3.84E−4	0.44	0.44	8.85E−5	0.15	3.07E−4	1.61	1.28
1.5	−3.76E−4	0.39	0.39	1.15E−4	0.19	2.74E−4	1.75	1.29
1.6	−3.61E−4	0.35	0.35	1.03E−4	0.18	2.79E−4	1.60	1.22

CoPi/Fe_2O_3								
Potential V_{RHE}	Accumulated lifetime			Dissipative lifetime				
	A_1 (ΔOD)	τ_1 (s)	$\tau_{average}$ (s)	A_1 (ΔOD)	τ_1 (s)	A_2 (ΔOD)	τ_2 (s)	$\tau_{average}$ (s)
0.6	—	—	—	—	—	—	—	—
0.7	−5.18E−5	2.42	2.42	—	—	5.38E−5	1.55	1.55
0.8	−4.64E−4	3.26	3.26	—	—	3.58E−4	2.81	2.8
0.9	−1.80E−3	3.77	3.77	—	—	1.32E−3	2.88	2.88
1.0	−2.47E−3	3.77	3.77	—	—	1.80E−3	2.88	2.88
1.1	−1.88E−3	1.89	1.89	—	—	1.65E−3	2.33	2.33
1.2	−1.50E−3	1.14	1.14	7.67E−5	0.23	1.30E−3	2.06	1.96
1.3	−1.36E−3	0.90	0.90	1.19E−4	0.14	1.16E−3	1.88	1.72
1.4	−1.33E−3	0.75	0.75	7.75E−5	0.15	1.14E−3	1.76	1.66
1.5	−1.27E−3	0.70	0.70	1.29E−4	0.17	1.04E−3	1.80	1.61
1.6	−1.22E−3	0.62	0.62	1.98E−4	0.23	9.38E−4	1.77	1.50

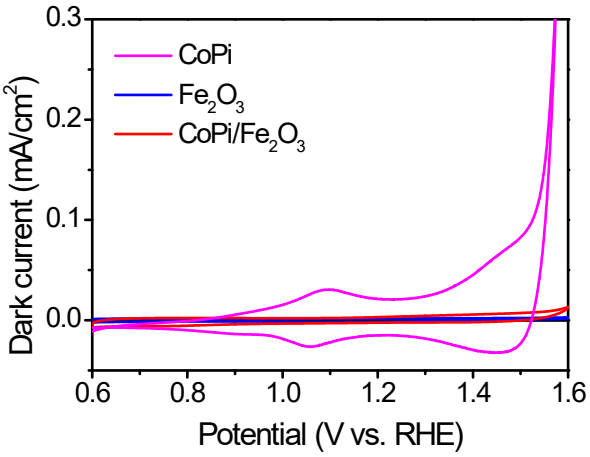

Fig. S1 CV curves for CoPi, bare Fe_2O_3 and CoPi/Fe_2O_3 anodes in dark.

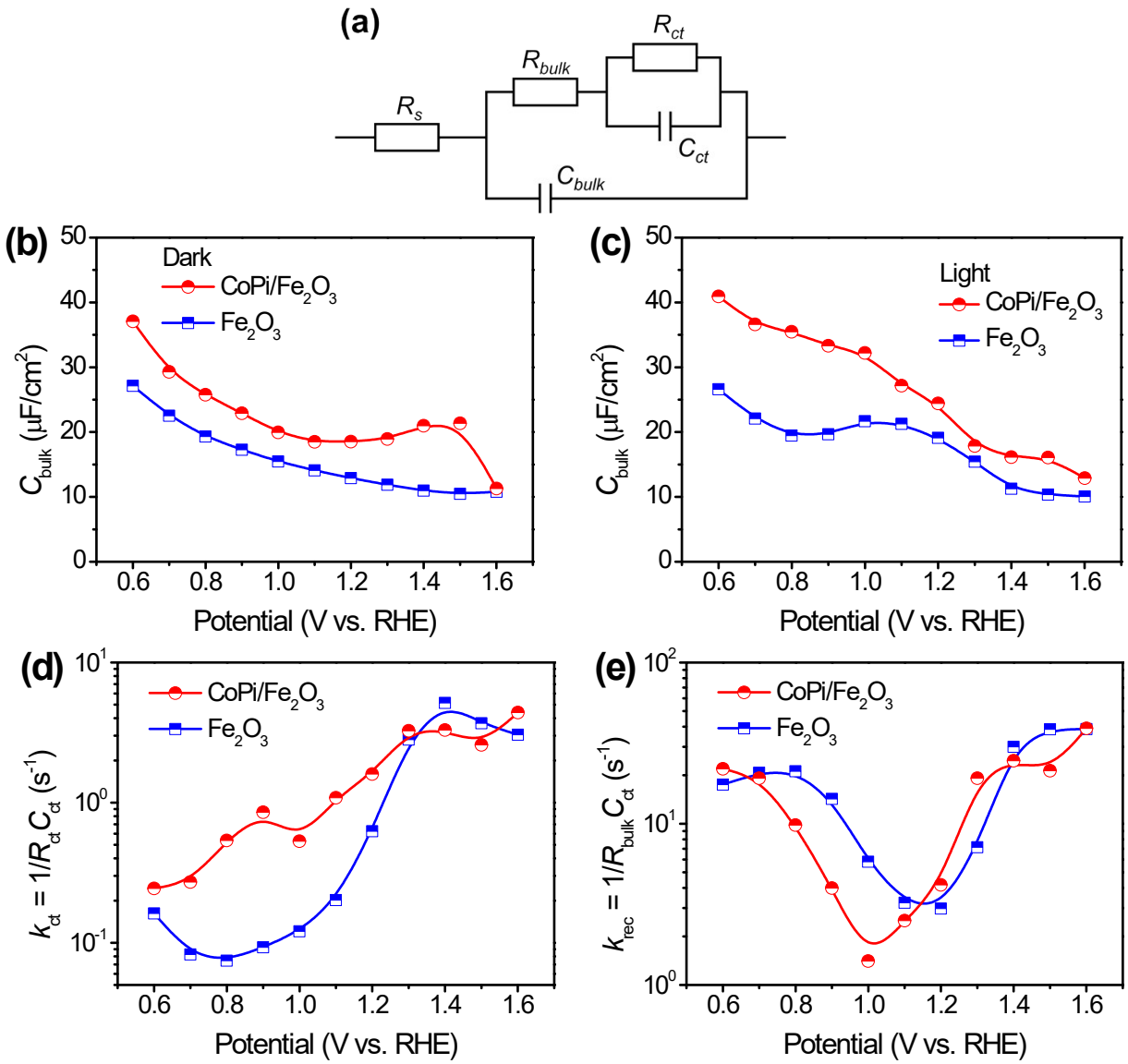

Fig. S2 EIS results for CoPi, Fe_2O_3 and CoPi electrodes. (a) Equivalent circuit. Bulk capacitance of in dark (b) and under illumination (c). Rate constants of charge transfer (d) and recombination (e) under illumination. Irradiation: 456 nm LED (5 mW/cm^2).

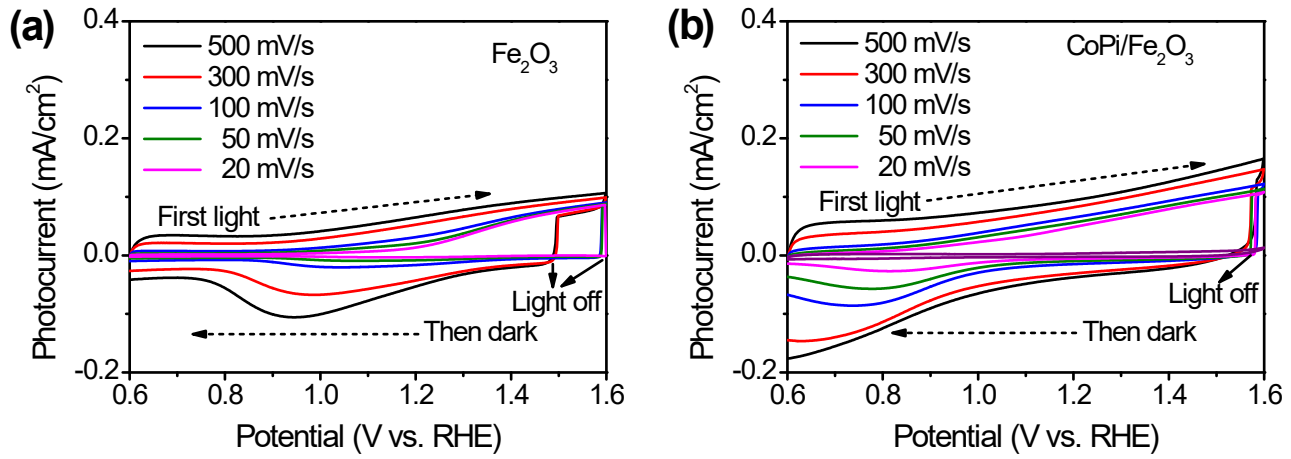

Fig. S3 CV of (a) bare Fe_2O_3 and CoPi/Fe_2O_3 photoanodes with different scan rates under illumination (first positive scan from low potential) and dark (following negative scan from high potential). Irradiation: 456 nm LED (5 mW/cm^2).

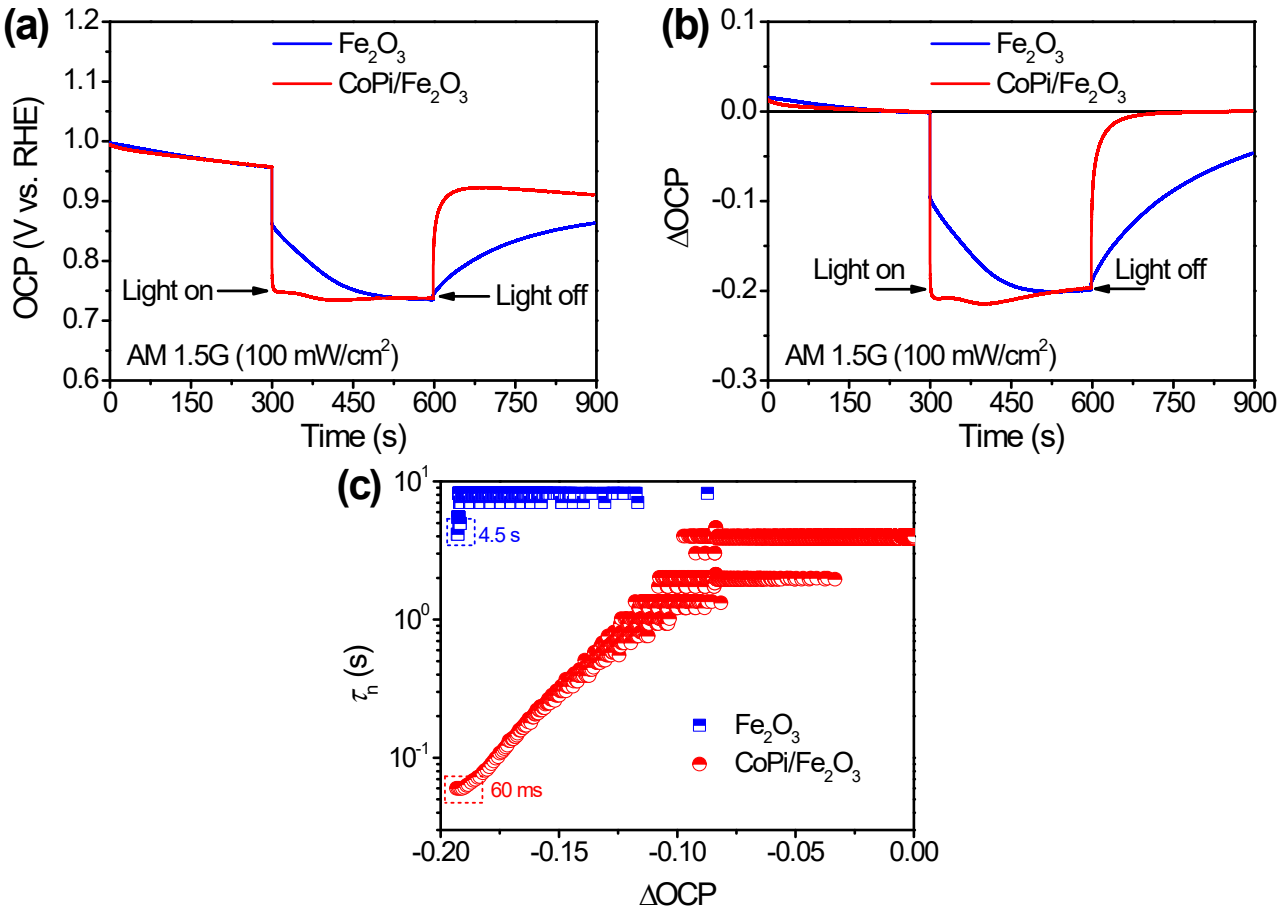

Fig. S4 The (a) raw and (b) corrected OCP with chopped light of bare Fe_2O_3 and $CoPi/Fe_2O_3$ photoanodes (illumination: AM 1.5G, 100 mW/cm^2). (c) Calculated decay life of OCP by function[11] of $\tau_n = \frac{k_B T}{e}\left(\frac{dOCP}{dt}\right)^{-1}$, where τ_n, k_B, T, e and $dOCP/dt$ are the carrier lifetime, Boltzmann's constant, temperature (K), charge of single electron and derivative of the OCP decay, respectively. The initial decay lifetimes (τ_0) after turning light off for Fe_2O_3 and $CoPi/Fe_2O_3$ are 4.5 s and 60 ms, respectively.

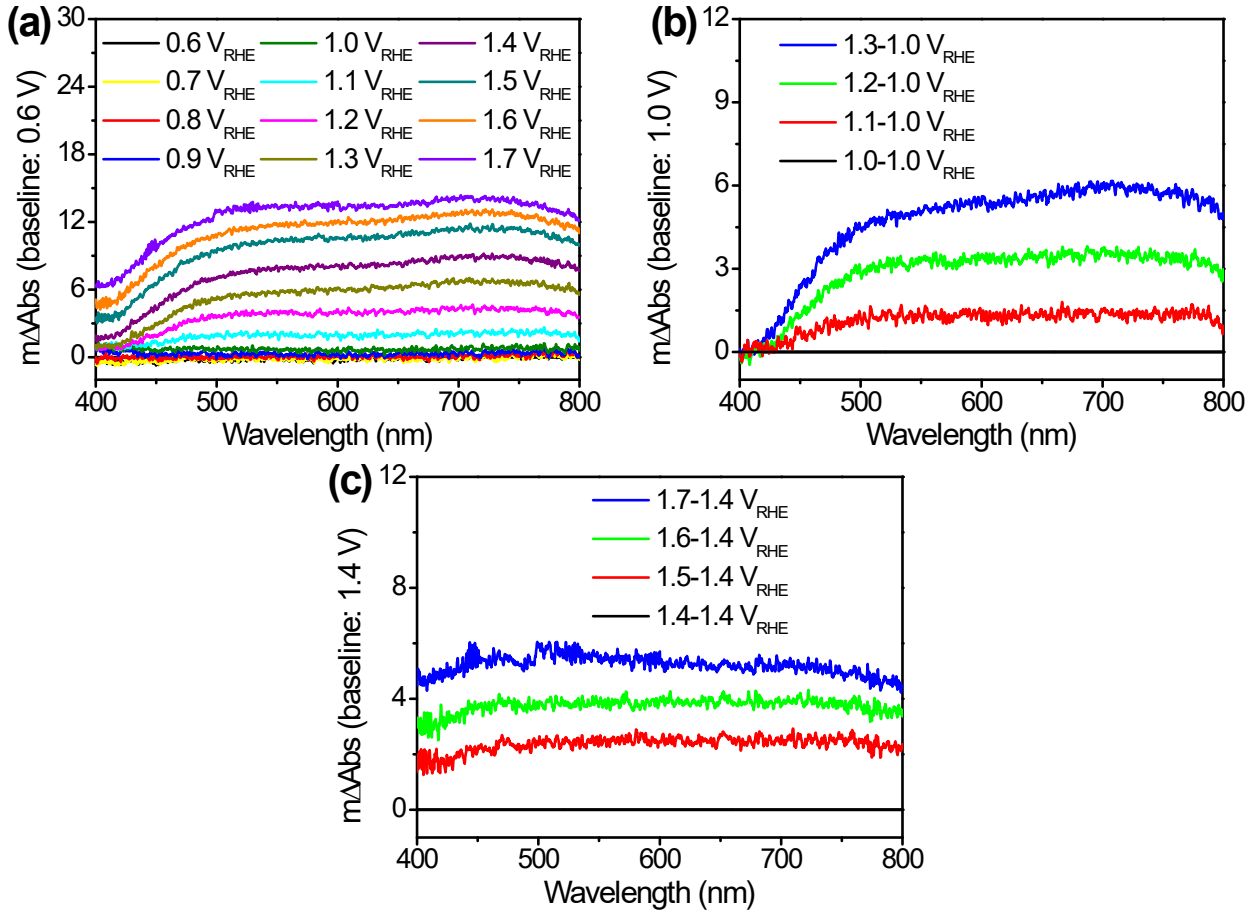

Fig. S5 SECA spectra of CoPi electrocatalyst at different baselines of (a) 0.6, (b) 1.0 and (c) 1.4 V_{RHE}. The baselines of 1.0 V_{RHE} and 1.4 V_{RHE} are used to identify the typical absorption spectra of $Co^{2+/3+}$ and $Co^{3+/4+}$ transition, respectively.

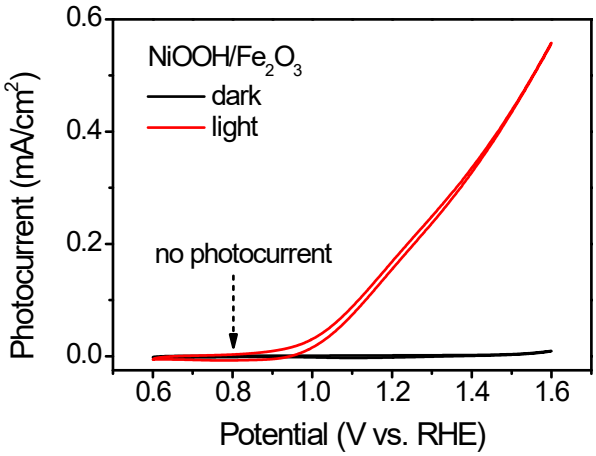

Fig. S6 CV of NiOOH/Fe_2O_3 photoanode with/without illumination (AM 1.5G: 100 mW/cm^2).

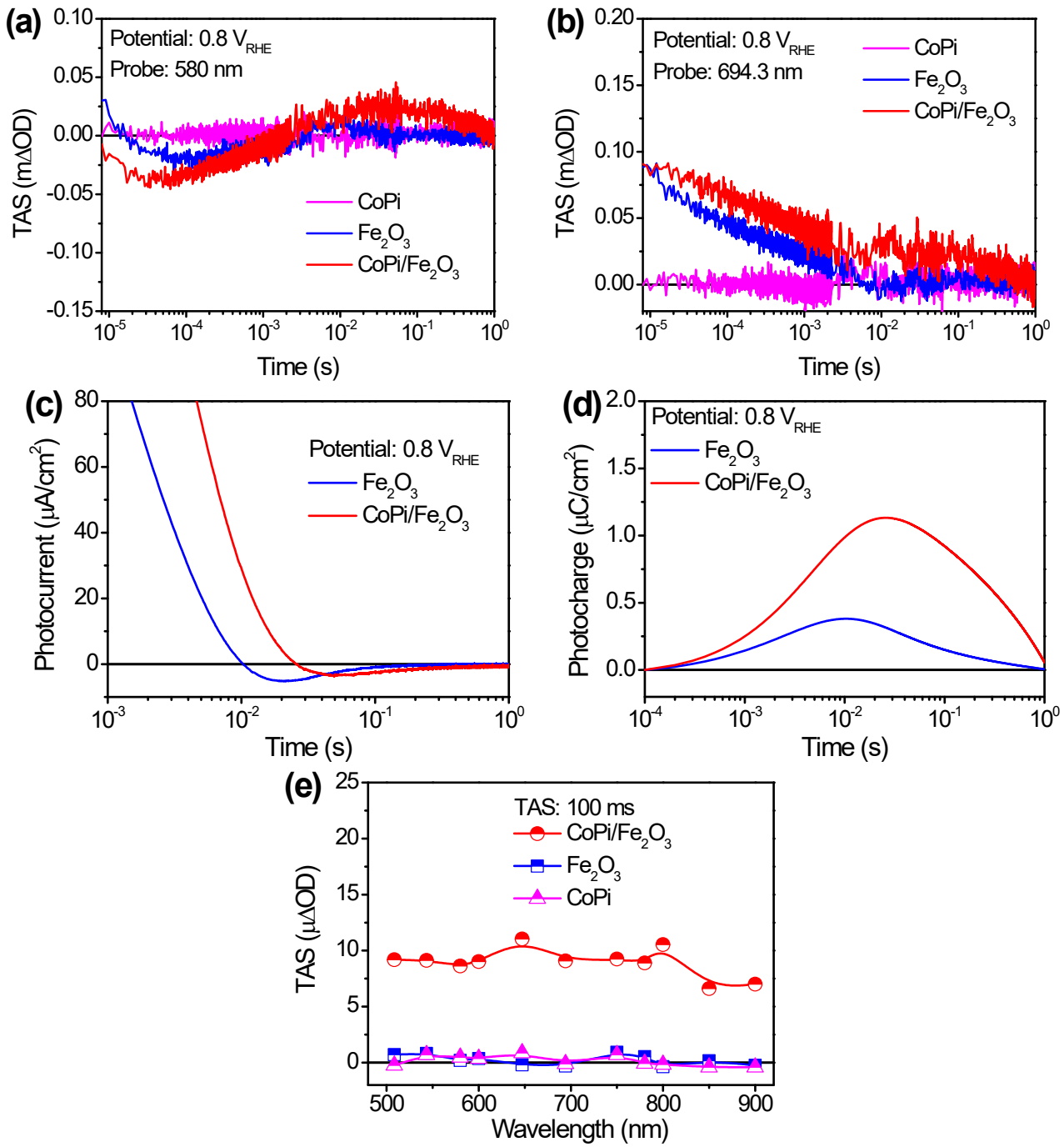

Fig. S7 TAS results at (a) 580 or (b) 694.3 nm of CoPi, bare Fe_2O_3 and CoPi/Fe_2O_3 photoanodes under 0.8 V_{RHE}. (c) TPC results and (d) integrated charge of bare Fe_2O_3 and CoPi/Fe_2O_3 photoanodes excited by nanosecond laser pulse under 0.8 V_{RHE}. (e) Transient absorption spectra at 100 ms of three electrodes at 0.8 V_{RHE}.

In Fig. S7e, transient absorption spectra at 100 ms at low applied potential of 0.8 V_{RHE} display a broad absorption which is quite similar to the absorption spectra of

oxidized Co^{3+} in Fig. S5b, demonstrating that the long-lived transient absorption signals in CoPi/Fe_2O_3 at lower potential should be originated from cobalt oxidation of $Co^{2+/3+}$. Moreover, this result demonstrates that cobalt oxidation by trapped holes starts occurring before 100 ms.

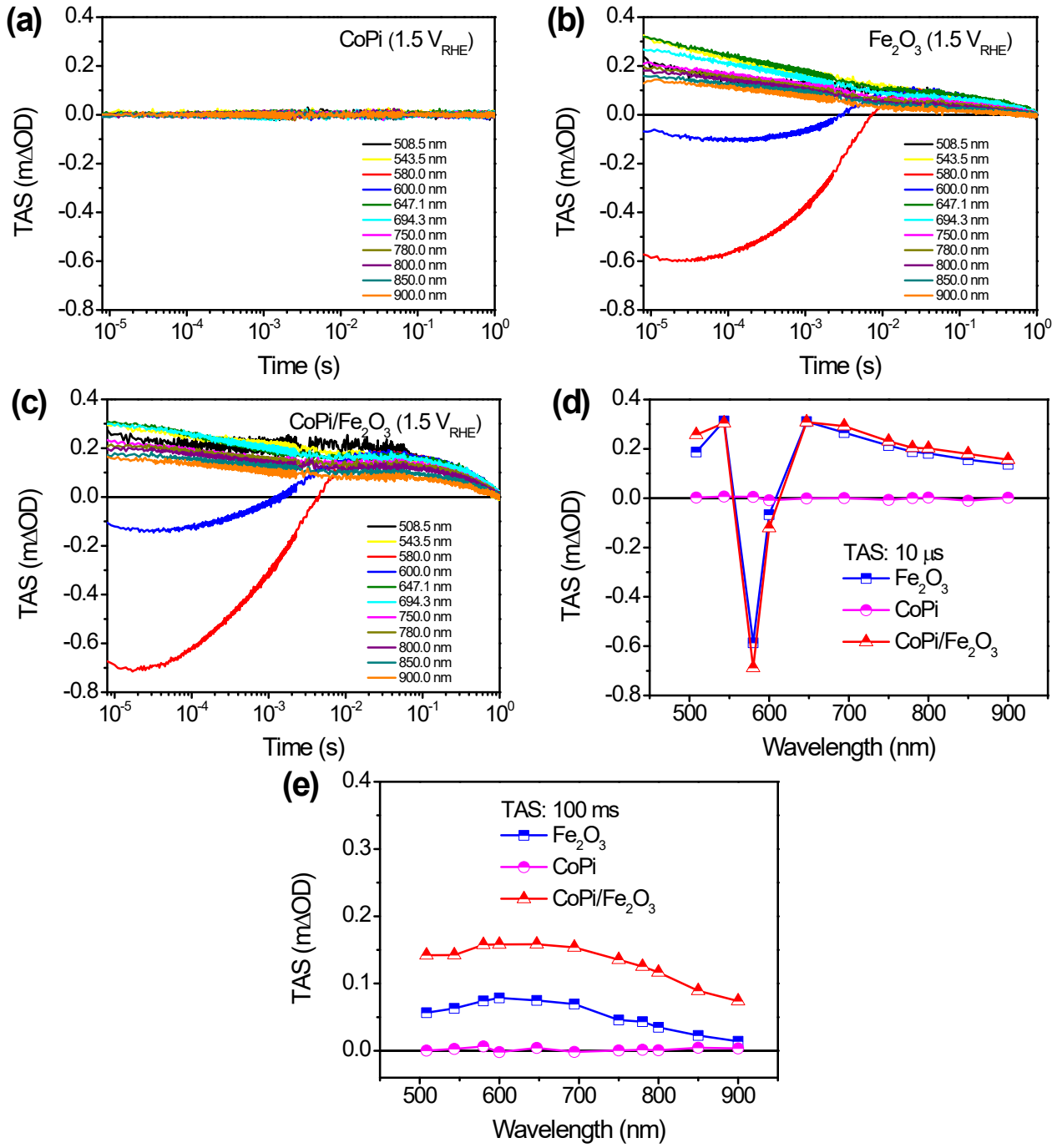

Fig. S8 TAS results of (a) CoPi, (b) bare Fe_2O_3 and (c) CoPi/Fe_2O_3 photoanodes under 1.5 V_{RHE}. Transient absorption spectra at (d) 10 μs and (e) 100 ms of three electrodes extracted from Figs. S8a−c.

Similar to PIA spectra, transient absorption spectra of CoPi/Fe_2O_3 photoanode at 100 ms at 1.5 V_{RHE} show similar spectra shape but higher amplitude relative to that of Fe_2O_3, demonstrating the same surface species. The higher TA amplitude of

CoPi/Fe_2O_3 at 100 ms demonstrates that the cobalt oxidation by VB holes starts occurring before 100 ms.

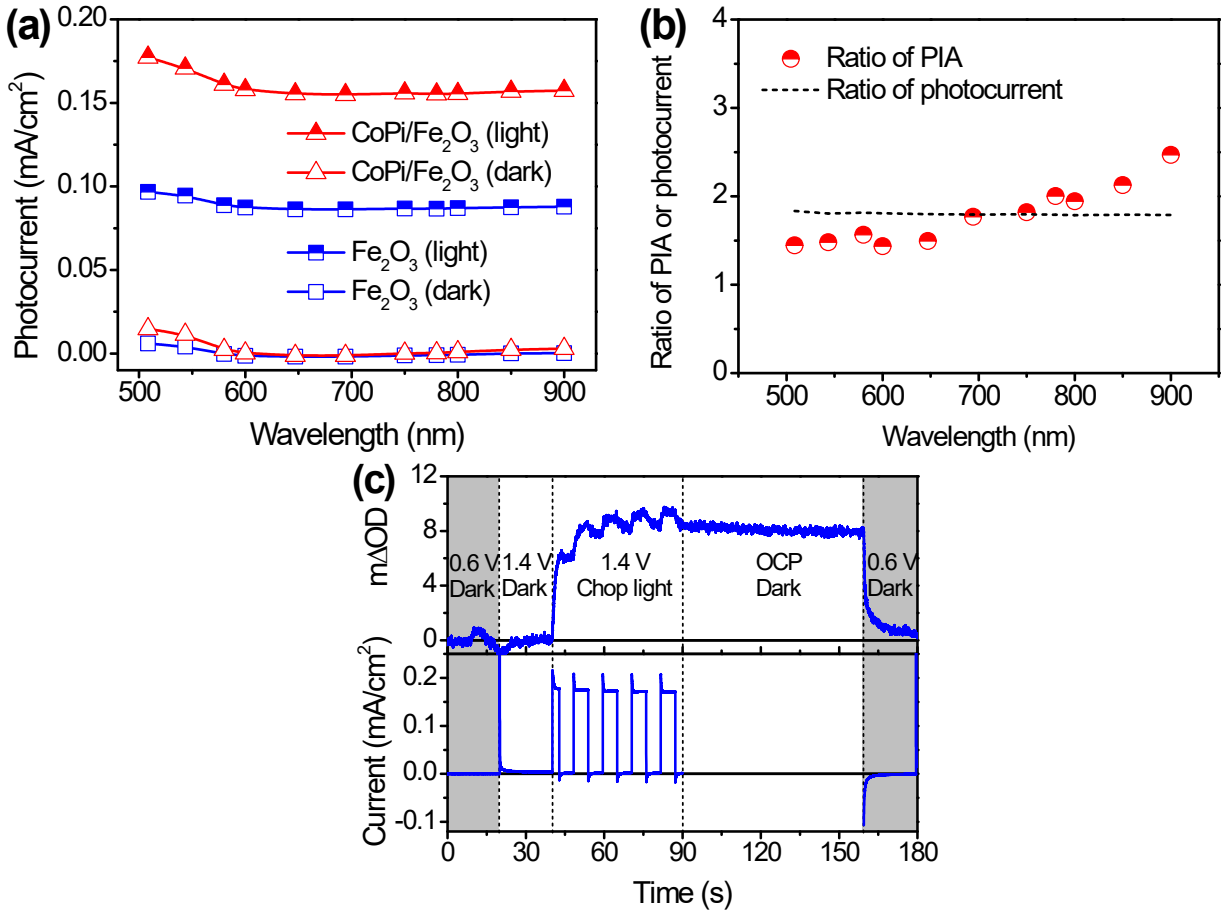

Fig. S9 (a) The corresponding photocurrents during PIA measurement for bare Fe_2O_3 and CoPi/Fe_2O_3 photoanodes. (b) The ratios of PIA amplitudes and photocurrents for bare Fe_2O_3 and CoPi/Fe_2O_3. (c) The change of PIA for CoPi/Fe_2O_3 photoanode at step potential and/or chop light. Pump: 456 nm (5 mW/cm^2); probe: 694.3 nm.

For CoPi/Fe_2O_3 photoanode, step potential from 0.6 V_{RHE} to 1.4 V_{RHE} in dark doesn't induce obvious change of optical density (Fig. S9c), which is in good agreement with the negligible dark current in CV of CoPi/Fe_2O_3 in Fig.S1. This result further confirms that the potential of 1.4 V_{RHE} cannot effectively oxidize loaded CoPi to Co^{3+} due to poor conductivity of dense Fe_2O_3. After applying chop light, a considerable increase of absorption amplitude is observed. Several light-dark cycles

will stabilize the optical density of CoPi/Fe_2O_3 at a quasi-steady-state state. These results should be due to the oxidation process of $Co^{2+/3+}$, since CoPi is oxidized to Co^{3+} via the sequential and direct hole transfer processes in light-dark cycle measurement (Fig. S9c). The oxidation of $Co^{2+/3+}$ is almost finished in about four light-dark cycles and stabilized in Co^{3+} states under 1.4 V_{RHE}. Since the PIA data in main text are quasi-steady-state PIA spectra measured with continuous pulsed light on, the initial states of cobalt ions in CoPi/Fe_2O_3 for PIA under 1.4 V_{RHE} should be Co^{3+} states.

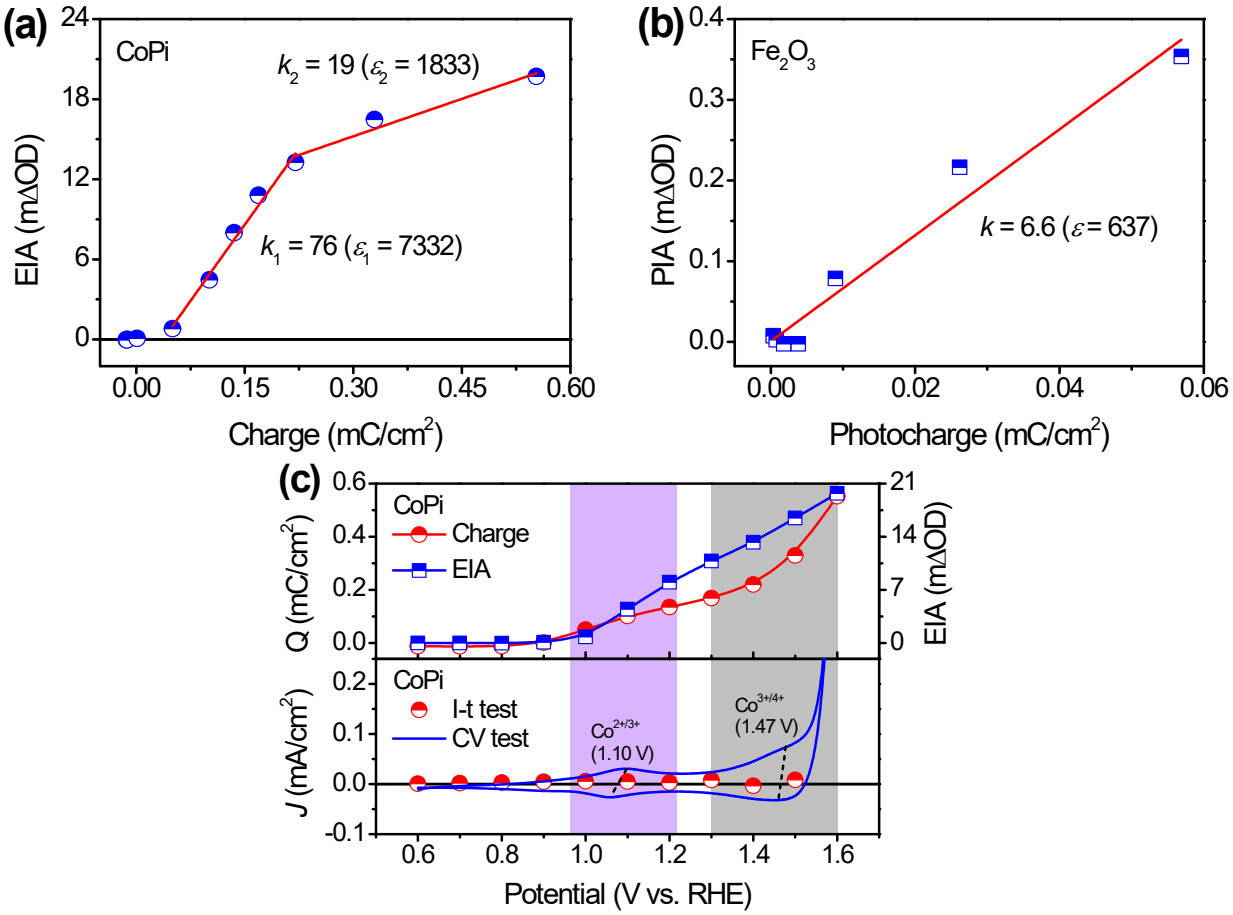

Fig. S10 Extinction coefficient of high-valent cobalt species in CoPi (a) and photoinduced holes in Fe_2O_3 (b) at probe wavelength of 694.3 nm. (c) Comparison of potential-dependent charges, EIA spectra, I-t and CV current for CoPi. Charges and EIA spectra were collected by step potential with 0.6 V_{RHE} baseline.

Extinction coefficient (ε) is calculated by linear relation between absorbance (ΔOD) at a specific wavelength (694.3 nm) and the concentration of charge (mC/cm^2), $\Delta OD = k \bullet c$, where the unit for slope k is $cm^2\ C^{-1}$.[10] By unit conversion, the extinction coefficient can be obtained from slope k: 1 ($cm^2\ C^{-1}$) = 96.48 $M^{-1}\ cm^{-1}$.

The concentration of high-valent cobalt species in CoPi and photoinduced holes in Fe_2O_3 is obtained by integrating the charge of multiple step potential measurement.

The spectroscopic intensity was collected by fixed potential baseline at 0.6 V_{RHE}. In Fig. S10a, CoPi shows two extinction coefficients, which are transition of $Co^{2+} \rightarrow Co^{3+}$ (ε_1 = 7,332 M^{-1} cm^{-1}) and $Co^{3+} \rightarrow Co^{4+}$ (ε_2 = 1,833 M^{-1} cm^{-1}), respectively. The transitions of both $Co^{2+} \rightarrow Co^{3+}$ and $Co^{3+} \rightarrow Co^{4+}$ induced by photoinduced holes in Fe_2O_3 will lead to increased spectroscopic absorption.

From Fig. S10a and S10c, Co^{4+} species in CoPi has been appeared with ~1.3 V_{RHE} potential and displays the second extinction coefficient. But the steady-state currents only appear above 1.5 V_{RHE}, illustrating that if Co^{4+} species participates in water oxidation reaction, it needs to accumulate a certain amount. When the accumulated amount is not enough, CoPi is only used to store holes but with weak reactivity.

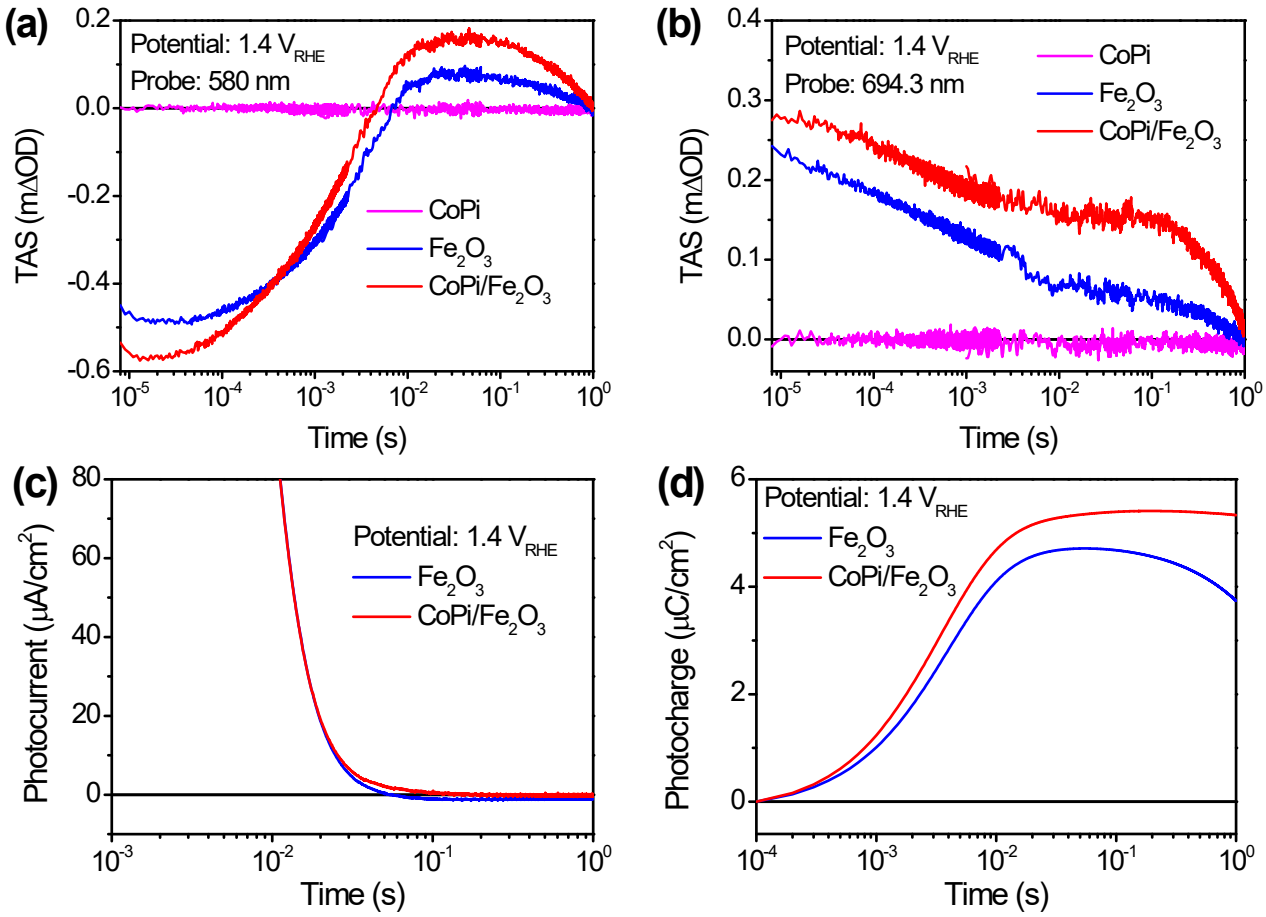

Fig. S11 TAS results at (a) 580 or (b) 694.3 nm of CoPi, bare Fe_2O_3 and CoPi/Fe_2O_3 photoanodes under 1.4 V_{RHE}. (c) (d) TPC results of bare Fe_2O_3 and CoPi/Fe_2O_3 photoanodes excited by nanosecond laser pulse under 1.4 V_{RHE}.

Above transient results excited by nanosecond laser pulse reproduce previous spectroscopic results of James R. Durrant group[3, 12]. Wherein, high potential will induce long-lived holes (positive absorption at 694.3 nm) on hematite surface and empty partially intrinsic electrons of trap states (negative absorption at 580 nm) in space charge region of hematite. Loading CoPi electrocatalyst can produce long-lived holes and empty intrinsic electrons under lower potential than pristine hematite. TPC results demonstrate that pristine hematite possesses severe back recombination

(negative TPC), which can be partially suppressed by loading CoPi electrocatalyst.

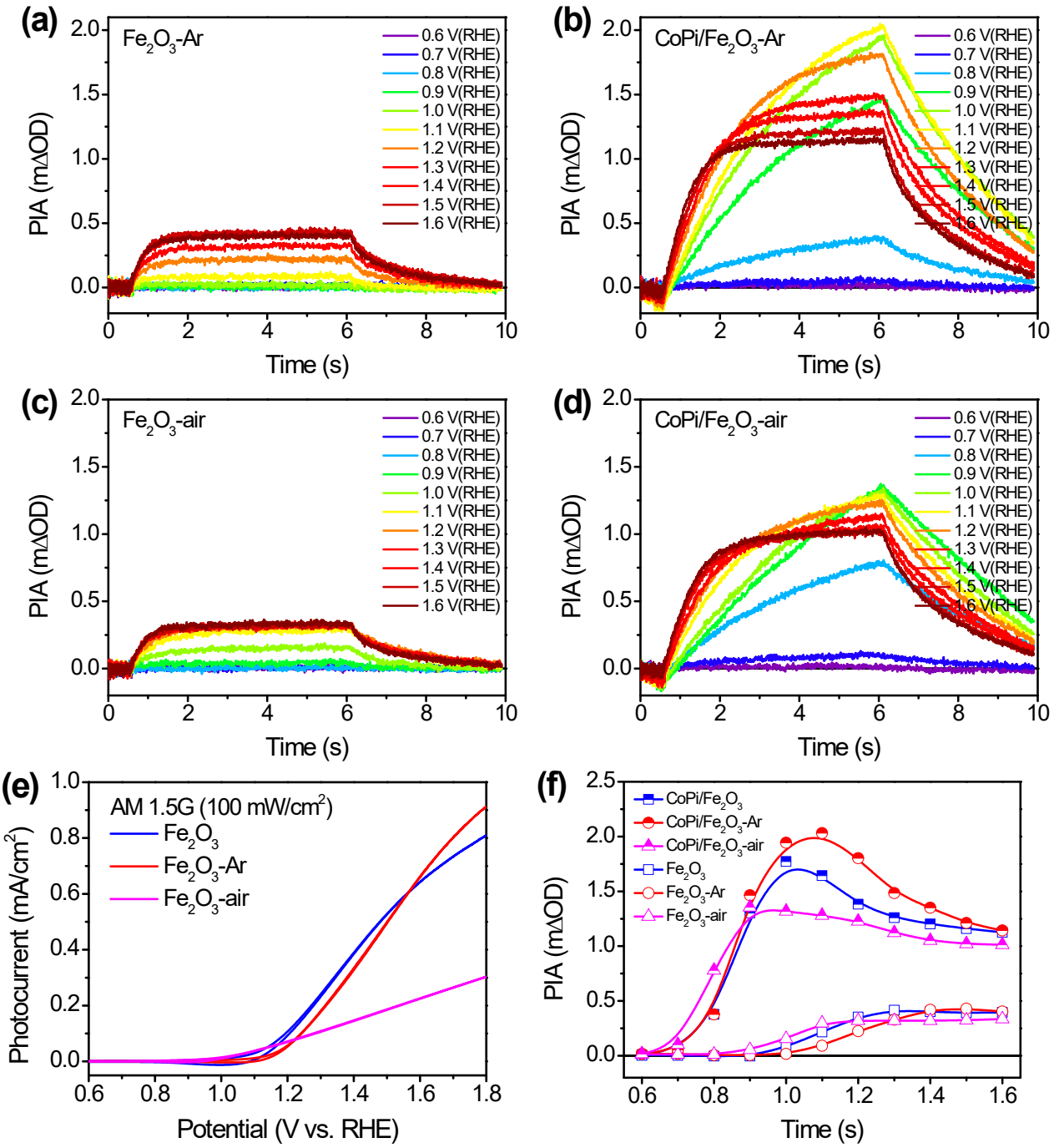

Fig. S12 Potential-dependent PIA responses under chopped illumination (blue LED: 456 nm, 5 mW/cm^2) for bare Fe_2O_3-Ar (a), CoPi/Fe_2O_3-Ar (b), bare Fe_2O_3-air (c) and CoPi/Fe_2O_3-air (d). (e) LSV curves for bare Fe_2O_3, Fe_2O_3-Ar and Fe_2O_3-air photoanodes under AM 1.5G illumination. (f) Potential-dependent PIA response for Fe_2O_3, Fe_2O_3-Ar and Fe_2O_3-air photoanodes under illumination of 456 nm (5 mW/cm^2). Probe wavelength: 694.3 nm.

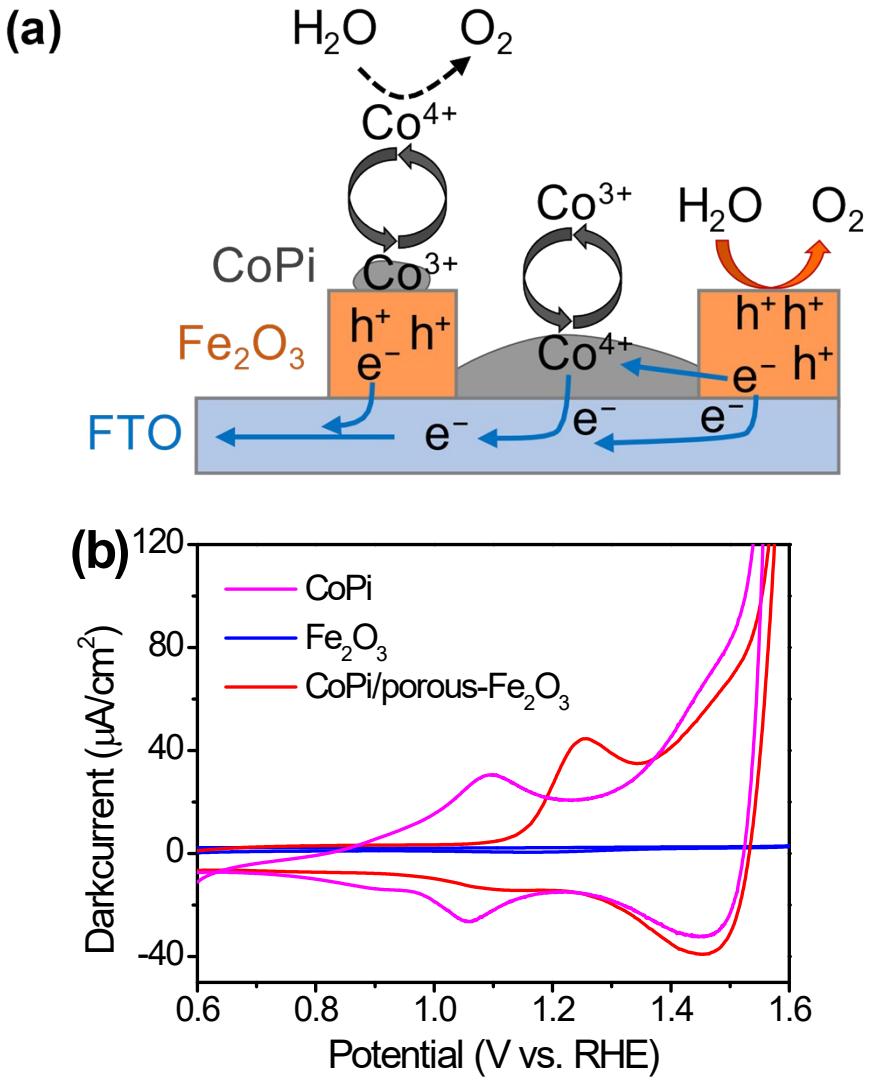

Fig. S13 (a) Schematic of contact between conductive substrate (FTO) and coating electrocatalyst (CoPi) resulting in electron shunt. (c) CV curves of porous Fe_2O_3 photoanodes with/without CoPi coating.

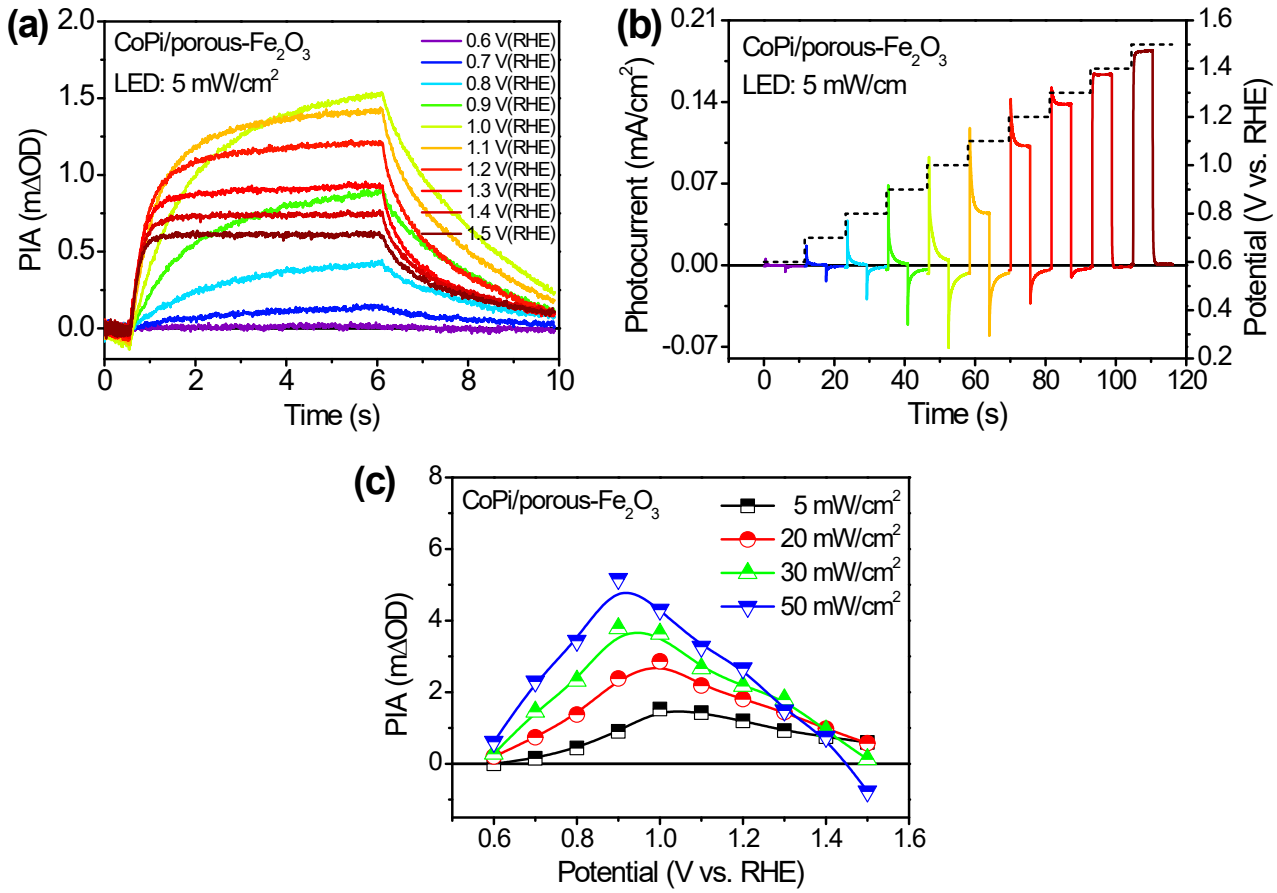

Fig. S14 (a) Potential-dependent PIA spectra and (b) chopped photocurrents for CoPi/porous-Fe_2O_3. Pump wavelength is 456 nm (5 mW/cm^2); probe wavelength is 694.3 nm; colors of curves at different potential in Fig. S14a and S14b are identical. (c) Light-intensity-dependent PIA spectra of porous Fe_2O_3 with loaded CoPi under increased potential.

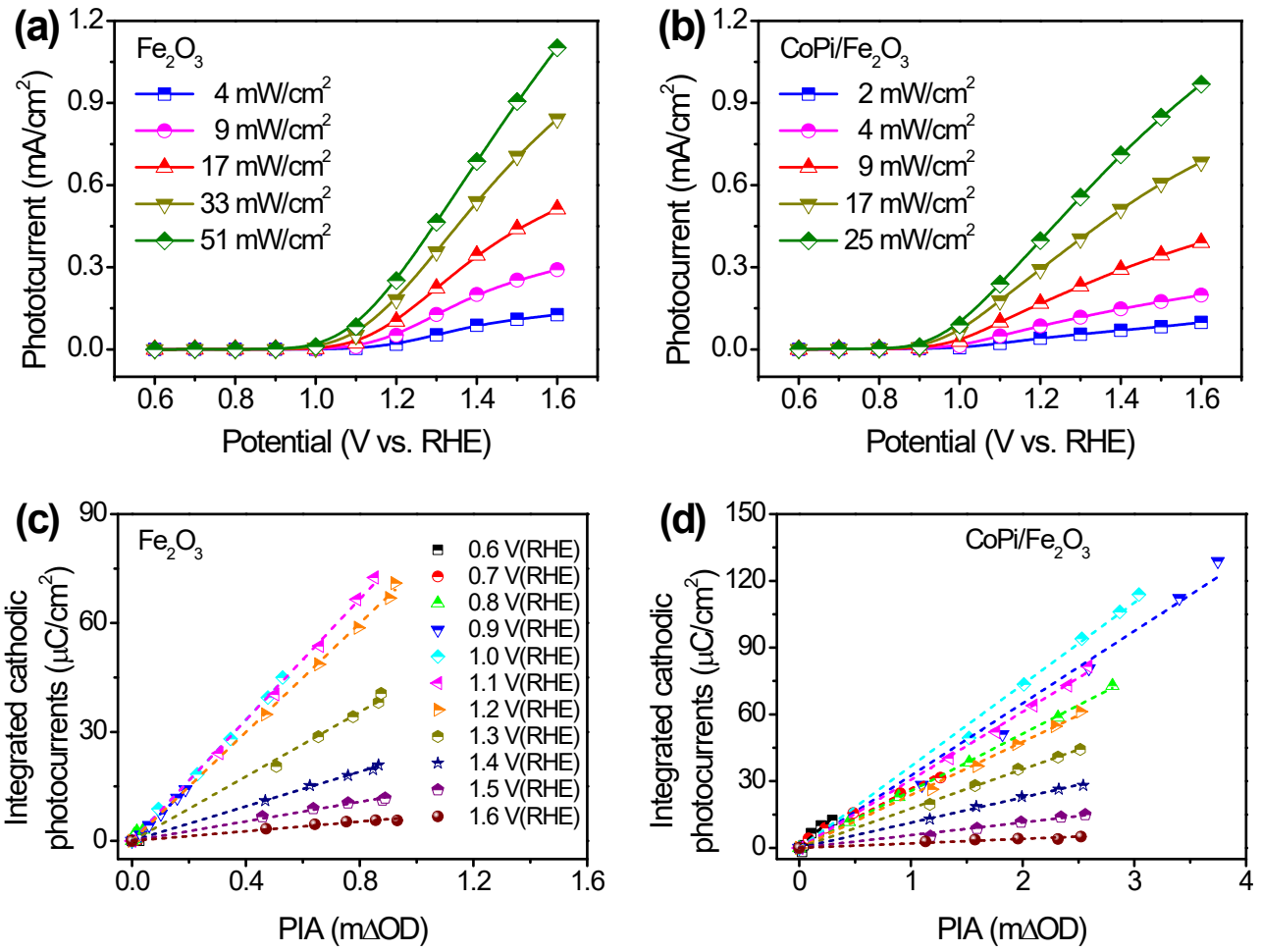

Fig. S15 The corresponding photocurrents during light-intensity-dependent PIA measurements for (a) bare Fe_2O_3 and (b) CoPi/Fe_2O_3 photoanodes. Linear relationship of PIA intensity and the integrated cathodic photocurrents for (c) bare Fe_2O_3 and (d) CoPi/Fe_2O_3 photoanodes. Colors of lines at different potential in Fig. S15a and S15b are identical.

According to the rate law ($J = k\cdot[h^+]^\beta$, $\log(J) = \log(k) + \beta\cdot\log([h^+])$), if two types of holes are present, rate law should be $\log(J) = \log(k) + \beta\cdot\log([h^+]_{active})$. PIA spectra concurrently monitor active and inactive holes, that's, $PIA_{total} = PIA_{active} + PIA_{inactive}$, where inactive holes are trapped holes of Fe_2O_3 and/or oxidized cobalt. The integrated

cathodic photocurrents from TPC results can be deemed as inactive hole density, because cathodic photocurrent spike is originated from back recombination.[13] The total PIA amplitudes and the integrated cathodic photocurrents show a linear relation at a fixed potential, as shown in Fig. S15c and S15d. Thus, $PIA_{inactive} = k_1 \cdot PIA_{total}$ ($0 < k_1 < 1$). Then, $PIA_{active} = (1 - k_1) \cdot PIA_{total}$. When PIA amplitude can be denoted to hole density, rate law is $\log(J) = \log(k') + \beta \cdot \log(PIA_{active}) = \log(k') + \beta \cdot \log((1 - k_1) \cdot PIA_{total}) = \log(k') + \beta \cdot \log(1 - k_1) + \beta \cdot \log(PIA_{total})$. Therefore, due to scaling relationship between total hole density and (in)active hole density at a fixed potential, the rate law analysis of Fe_2O_3 and $CoPi/Fe_2O_3$ photoanodes is valid.

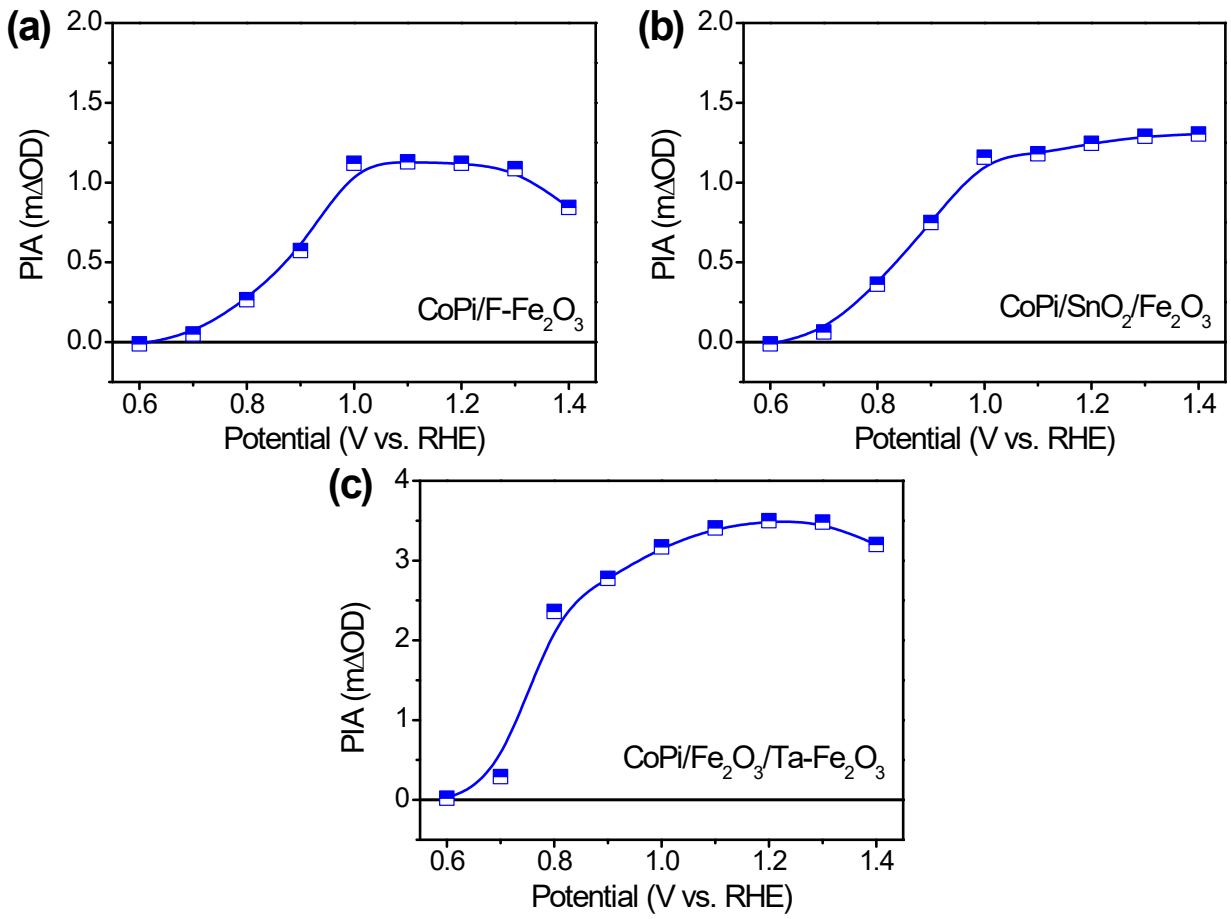

Fig. S16 Potential-dependent PIA response of four CoPi-modified hematite photoanodes. (a) CoPi/F-Fe_2O_3, (b) CoPi/SnO_2/Fe_2O_3 and (c) CoPi/Fe_2O_3/Ta-Fe_2O_3. Pump wavelength is 456 nm (5 mW/cm^2) and probe wavelength is 694.3 nm.

The adverse recombination processes of surface states will be released by several strategies influencing photogenerated electrons on/near hematite surface. In Fig. S16a, deceasing density of surface states by surface covalent doping with fluorine (CoPi/F-Fe_2O_3) induces a platform of PIA response at 1.0−1.3 V_{RHE} instead of the PIA peak in CoPi/Fe_2O_3. After surface insulator modification on hematite surface (CoPi/SnO_2/Fe_2O_3) in Fig. S16b, the reverse electron transfer between Fe_2O_3 and CoPi will be greatly suppressed due to blocking of SnO_2, resulting in gradually increasing

PIA intensity in potential-dependent PIA response in line with monodirectional hole transfer process. In addition, since constructing build-in electric field near Fe_2O_3 surface ($CoPi/Fe_2O_3/Ta\text{-}Fe_2O_3$) can drive surface photoinduced electrons into Fe_2O_3 bulk, a delayed PIA peak at 1.2~1.3 V_{RHE} is observed. From the potential-dependent PIA response of three CoPi-modified hematite photoanodes in Fig. S16, three strategies do achieve the aim that regulating surface states will influence surface recombination processes. Wherein, disappeared PIA peak for $CoPi/SnO_2/Fe_2O_3$ photoanode illustrates that the back recombination processes are strongly suppressed.

References

1. J. Y. Kim, D. H. Youn, K. Kang and J. S. Lee, *Angew. Chem. Int. Ed.*, 2016, **55**, 10854-10858.
2. Z. Wang, G. Liu, C. Ding, Z. Chen, F. Zhang, J. Shi and C. Li, *J. Phys. Chem. C*, 2015, **119**, 19607-19612.
3. M. Barroso, C. A. Mesa, S. R. Pendlebury, A. J. Cowan, T. Hisatomi, K. Sivula, M. Gratzel, D. R. Klug and J. R. Durrant, *Proc. Natl. Acad. Sci. U. S. A.*, 2012, **109**, 15640-15645.
4. C. G. Morales-Guio, L. Liardet and X. Hu, *J. Am. Chem. Soc.*, 2016, **138**, 8946-8957.
5. Z. Wang, X. Mao, P. Chen, M. Xiao, S. A. Monny, S. Wang, M. Konarova, A. Du and L. Wang, *Angew. Chem. Int. Ed.*, 2019, **58**, 1030-1034.
6. S. Chen, J. Bai, X. Nurimaimaiti, J. Wang, Y. Zhang, T. Zhou, J. Li and B. Zhou, *Nano Energy*, 2020, **78**.
7. H. Zhang, D. Li, W. J. Byun, X. Wang, T. J. Shin, H. Y. Jeong, H. Han, C. Li and J. S. Lee, *Nat. Commun.*, 2020, **11**, 4622.
8. T. Hisatomi, H. Dotan, M. Stefik, K. Sivula, A. Rothschild, M. Gratzel and N. Mathews, *Adv. Mater.*, 2012, **24**, 2699-2702.
9. H. Yin, D. Li, X. Wang and C. Li, *J. Phys. Chem. C*, 2021, **125**, 8369-8375.
10. L. Francas, S. Corby, S. Selim, D. Lee, C. A. Mesa, R. Godin, E. Pastor, I. E. L. Stephens, K. S. Choi and J. R. Durrant, *Nat. Commun.*, 2019, **10**, 5208.

11. J. Bisquert, A. Zaban, M. Greenshtein and I. Mora-Seró, *J. Am. Chem. Soc.*, 2004, **126**, 13550-13559.

12. F. Le Formal, S. R. Pendlebury, M. Cornuz, S. D. Tilley, M. Gratzel and J. R. Durrant, *J. Am. Chem. Soc.*, 2014, **136**, 2564-2574.

13. J. Li, W. Wan, C. A. Triana, Z. Novotny, J. Osterwalder, R. Erni and G. R. Patzke, *J. Am. Chem. Soc.*, 2019, **141**, 12839-12848.